Nicotinic Receptor Interloop Proline Anchors β1-β2 and Cys loops in Coupling Agonist Binding to Channel Gating

Won Yong Lee, Chris R. Free, and Steven M. Sine

Receptor Biology Laboratory, Department of Physiology and Biomedical Engineering, Mayo Clinic College of Medicine, Rochester, MN 55905

Nicotinic acetylcholine receptors (AChRs) mediate rapid excitatory synaptic transmission throughout the peripheral and central nervous systems. They transduce binding of nerve-released ACh into opening of an intrinsic channel, yet the structural basis underlying transduction is not fully understood. Previous studies revealed a principal transduction pathway in which αArg 209 of the pre-M1 domain and αGlu 45 of the β1–β2 loop functionally link the two regions, positioning αVal 46 of the β1–β2 loop in a cavity formed by αPro 272 through αSer 269 of the M2–M3 loop. Here we investigate contributions of residues within and proximal to this pathway using single-channel kinetic analysis, site-directed mutagenesis, and thermodynamic mutant cycle analysis. We find that in contributing to channel gating, αVal 46 and αVal 132 of the signature Cys loop couple energetically to αPro 272. Furthermore, these residues are optimized in both their size and hydrophobicity to mediate rapid and efficient channel gating, suggesting naturally occurring substitutions at these positions enable a diverse range of gating rate constants among the Cys-loop receptor superfamily. The overall results indicate that αPro 272 functionally couples to flanking Val residues extending from the β1–β2 and Cys loops within the ACh binding to channel opening transduction pathway.

The Journal of General Physiology

INTRODUCTION

During neuromuscular transmission, quantal release of acetylcholine (ACh) activates ACh receptor (AChR)–coupled ion channels, which depolarize the muscle cell, trigger an action potential, and ultimately cause muscle contraction. The central task of the AChR is to transduce binding of ACh into opening of a narrow pore some 50 Å away. For more than a decade it has been possible to detect and quantify elementary reaction steps underlying ACh binding and gating of the pore, but the structural bases for the two processes and how they are linked are not fully understood (Sine and Engel, 2006). However, recent x-ray structures of ACh-binding proteins (AChBP) at resolutions from 2 to 3.4 Å (Brejc et al., 2001; Hansen et al., 2005) and the cryoelectron microscopic structural model of the *Torpedo* AChR at 4 Å (Unwin, 2005) allow unprecedented development of hypotheses that can be tested by a battery of structural, functional and computational approaches.

Each of the five AChR subunits consists of an extracellular domain composed mainly of β sheets, four transmembrane α helices (M1–M4) and a cytoplasmic domain containing substantial α-helix (Unwin, 2005). The two ACh binding sites are located within the extracellular domain, at the junctions of the α and either the ε or the δ subunits, while the narrow constriction of the pore is formed by M2 from all five subunits. Computational and experimental studies of AChBP and of the AChR reveal dynamic structural changes of the binding site associated with agonist occupancy: in the resting state, a hairpin structure called the C-loop adopts an uncapped conformation, allowing agonist to enter the aromatic-rich binding pocket, but in the presumed active state the C-loop assumes a capped conformation that envelops the agonist within the pocket (Sine and Engel, 2006). β strands from the C-loop extend to the junction of the ligand binding and pore domains where they are poised to propagate the capping motion to the pore. Within the binding pore junction, three loops and an interdomain connector from the ligand binding domain (β1–β2 loop, Cys loop, β8–β9 loop, pre-M1 strand) merge with the interhelical M2–M3 loop from the pore domain. Within this junction, the invariant αArg 209 from the pre-M1 strand joins the highly conserved αGlu 45 from the β1–β2 loop, and the resulting interdomain assembly overlays the interhelical M2–M3 loop. In the muscle (Lee and Sine, 2005) and ρ1 GABA receptors (Wang et al., 2007), charge reversal experiments provided evidence that this salt bridge is a principal conduit functionally linking the binding and pore domains. However, in addition to the salt bridge, flanking hydrophobic residues are also required for rapid and efficient coupling

Correspondence to Steven M. Sine: sine@mayo.edu

Abbreviations used in this paper: AChR, acetylcholine receptor; NMA, Normal mode analyses; REFER, rate-equilibrium free energy relationship.

The Rockefeller University Press $30.00
J. Gen. Physiol. Vol. 132 No. 2 265–278
www.jgp.org/cgi/doi/10.1085/jgp.200810014

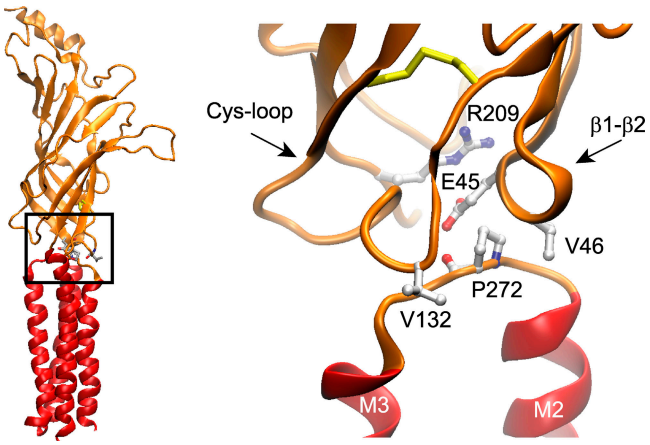

Figure 1. Structural model of the α-subunit from the *Torpedo* AChR (PDB code 2BG9) highlighting the binding-pore interface (boxed region, left; higher magnification, right). αPro 272 of the M2–M3 loop is flanked by αGlu 45 and αVal 46 of the β1–β2 loop and αVal 132 of the Cys loop. Side chains are shown in ball-and-stick representation and colored according to the electronic charge (blue, positive; red, negative; and gray, neutral). The signature αCys 128/αCys 142 disulfide bond is colored yellow.

of agonist binding to channel gating (Chakrapani et al., 2003; Chakrapani and Auerbach, 2005; Grutter et al., 2005; Lee and Sine, 2005).

Here we use single-channel kinetic analysis, site-directed mutagenesis, and thermodynamic mutant cycle analysis to examine structural bases for the functional contributions of three hydrophobic residues that flank the key salt bridge. We find that αVal 132 of the signature Cys loop, αVal 46 the β1–β2 loop, and αPro 272 within the M2–M3 linker are optimized to provide the proper hydrophobicity and steric fit required for rapid and efficient channel gating. The findings further suggest that in transducing ACh binding into channel opening, αPro 272 serves as an anchor that joins the pair of Val residues from the β1–β2 and Cys loops.

MATERIALS AND METHODS

Construction of Wild-Type and Mutant AChRs

Human α, β, δ, and ε-subunit cDNAs were subcloned in the CMV-based mammalian expression vector pRBG4 (Lee et al., 1991), as described previously (Ohno et al., 1996). Site-directed mutations were made using the QuickChange site-directed mutagenesis kit (Stratagene). The presence of each mutation and the absence of unwanted mutations were confirmed by sequencing the entire cDNA insert.

Mammalian Cell Expression

All experiments were performed using the BOSC 23 cell line (CRL-11270, American Type Culture Collection), a variant of the HEK 293 cell line. Cells were maintained in the Dulbecco's modified Eagle medium containing FBS (10% vol/vol) at 37°C until they reached ~50–70% confluence. Wild-type or mutant AChR cDNAs plus cDNA encoding green fluorescent protein were then transfected by calcium-phosphate precipitation using final concentrations of each cDNA of 0.68 μg/ml. Patch-clamp recordings were performed 1–2 d after transfection.

Patch-Clamp Single-Channel Recordings

To record single-channel currents, cells transfected with wild-type or mutant AChR cDNAs were rinsed with and maintained in the following bath solution (in mM): KCl 142, NaCl 5.4, $CaCl_2$ 1.8, $MgCl_2$ 1.7, and HEPES 10 (pH was adjusted to 7.4 with NaOH). The same solution was used to fill patch pipettes. ACh (Sigma-Aldrich) was kept as a 10 mM stock in bath solution and stored at −80°C until use. Glass micropipettes (type 7052; Garner Glass Co.) were coated with Sylgard 184 (Dow Corning Co.) and heat polished to yield resistances of 5–8 MΩ. After identifying transfected cells under fluorescence optics, single-channel currents were recorded in the cell-attached configuration at 22°C using the Axopatch 200A (Axon Instruments, Inc.) at a holding membrane potential of −70 mV. Data were collected from two to four different patches for each ACh concentration, choosing only recordings in which channel activity was low enough to allow clear identification of activation episodes resulting from a single channel. The current signal was low pass filtered at 50 kHz and recorded to hard disk at 200 kHz using the program Acquire (Bruxton Co.). Recording of single-channel currents over a range of ACh concentrations from each mutant receptor was done within 12 h.

Single-Channel Kinetic Analysis

Detailed methods of single-channel kinetic analyses were described previously (Lee and Sine, 2004). In brief, the digitized current signal was filtered using a 10-kHz digital Gaussian filter (Colquhoun and Sigworth, 1983). Channel events were detected by the half-amplitude threshold criterion using the program TAC with an imposed dead time of 10 μs (Bruxton Co.). Precise determination of each dwell time at threshold was achieved by cubic spline interpolation of the digital signal and the measured dwell time at threshold was corrected for the effects of the Gaussian filter (Colquhoun and Sigworth, 1983). Open and closed time histograms were fitted by the sum of exponentials by maximal likelihood using the program TACFit (Bruxton Co.). Openings corresponding to a single receptor channel were identified by assigning a critical closed time defined as the point of intersection of the closed time component that depended on ACh concentration with the succeeding concentration-independent component (Ohno et al., 1996), presumed due to fast desensitization. Because this method removes most, but not all, closed dwell times due to fast desensitization, analyses were also performed in which the critical closed time was defined as the intersection of the closed time component due to fast desensitization with the succeeding component, and the scheme modified to include a desensitized state connected to the doubly occupied open state. To obtain kinetically homogeneous data, defined single-channel episodes containing at least five openings were analyzed for channel open probability, mean open time, and mean closed time, and episodes within two standard deviations of the mean were accepted for further analysis (Wang et al., 1997). It should be mentioned that this processing removes a small population of single brief openings flanked by long closed periods (Sine and Steinbach, 1987). For the receptors examined in this study, the overall selection retained greater than 80% of the detected single-channel events. The kinetic scheme was fitted simultaneously to all the data obtained across a range of ACh concentrations (global fit) using MIL software (QuB suite, State University of New York, Buffalo, NY), which employs a maximum likelihood optimization criterion, corrects for missed events, and gives error estimates of the fitted parameters (Qin et al., 1996). An instrument dead time of 22 μs was uniformly applied to all recordings. For a given wild-type or mutant receptor, our global analysis included data from two to four patches for each ACh concentration, with the ACh concentrations spaced at half log-unit intervals over a two to three log-unit range of concentration. For each receptor mutant, the range of the ACh concentration spanned from the minimum to the maximum channel open probability.

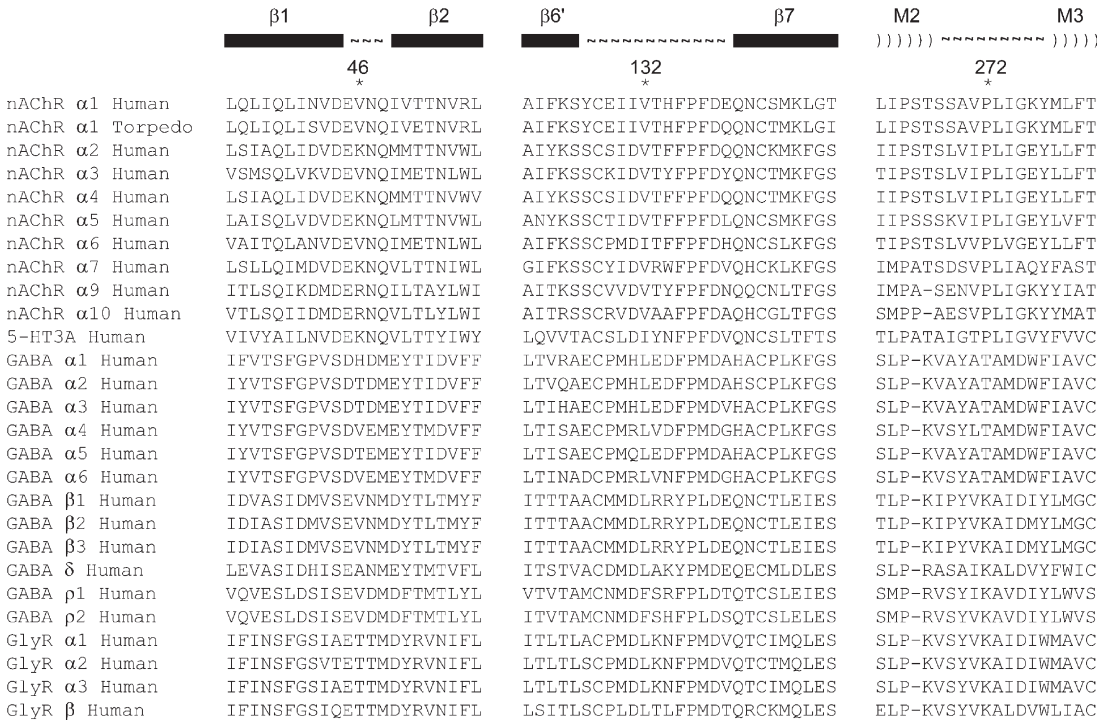

Figure 2. Sequence alignment of subunits from the Cys-loop receptor superfamily. Secondary structural regions are shown at the top, with residue positions equivalent to αVal 46, αVal 132, and αPro 272 indicated by asterisks.

The following kinetic scheme was fitted to the single-channel open and closed dwell times:

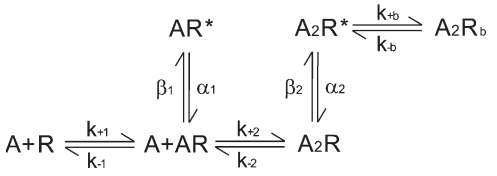

Two ACh (A) molecules associate with the receptor (R) with rate constants k_{+1} and k_{+2}, and dissociate with rate constants k_{-1} and k_{-2}. Occupied closed receptors (AR and A_2R) produce singly (AR*) and doubly occupied (A_2R*) open states that close with rate constants α_1 and α_2. Rate constants for open channel blocking (k_{+b}) and unblocking (k_b) by ACh are included.

Double Mutant Cycle Analysis

To detect inter-residue energetic coupling and estimate its magnitude, we applied mutant cycle analysis (Carter et al., 1984; Kellis et al., 1988; Hidalgo and MacKinnon, 1995) to the di-liganded gating equilibrium constant Θ_2, computed from the ratio of rate constants β_2/α_2 (Lee and Sine, 2005). The following mutant cycle examines energetic coupling between two residues 1 and 2 for which substitutions alter a functional parameter such as the channel gating equilibrium constant examined in the current study.

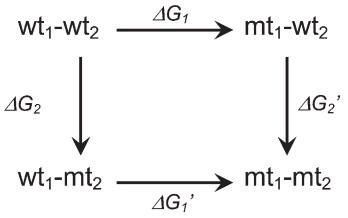

For each substitution, the change in Θ_2 relative to that of the wild-type AChR is expressed as $\Delta G = -RT\ln(\Theta_2 mt/\Theta_2 wt)$, where R is the gas constant and T the absolute temperature. If two residues are functionally or structurally independent, mutation of residue 1 will cause equivalent changes in gating free energy whether residue 2 contains a wild-type or mutant residue: $\Delta G_1 = \Delta G_1'$ and $\Delta G_2 = \Delta G_2'$. Conversely, if residues 1 and 2 are interdependent, $\Delta G_1 \neq \Delta G_1'$ and $\Delta G_2 \neq \Delta G_2'$. While the sum of the free energy changes along either pathway of the cycle are equal, that is, $\Delta G_1 + \Delta G_2' = \Delta G_1' + \Delta G_2$, interdependent residues will show a coupling energy $\Delta\Delta G_{int} = (\Delta G_1 - \Delta G_1', \Delta G_2 - \Delta G_2') \neq 0$.

RESULTS

Nonconserved Residues Proximal to the Principal Pathway

The interface of the ligand binding and pore domains is depicted in the structural model of the *Torpedo* AChR α-subunit at a resolution of 4 Å (Fig. 1; PDB 2BG9; Unwin, 2005). Located within this interface is the principal coupling pathway that functionally links the two domains. The charge pair, αArg 209 and αGlu 45, is conserved across the Cys-loop superfamily in eukaryotes, but residues near this pair are not conserved. The position equivalent to αVal 46 of the β1–β2 loop can be substituted by Lys, Arg, Ala, Thr, or His; the position equivalent to αVal 132 of the Cys loop can be substituted by Ile, Leu, or Phe; and αPro 272 of the M2–M3 loop can be substituted by Lys or Thr (Fig. 2). The diversity of residues at the three positions suggests differences in the local structure flanking the principal coupling pathway contribute

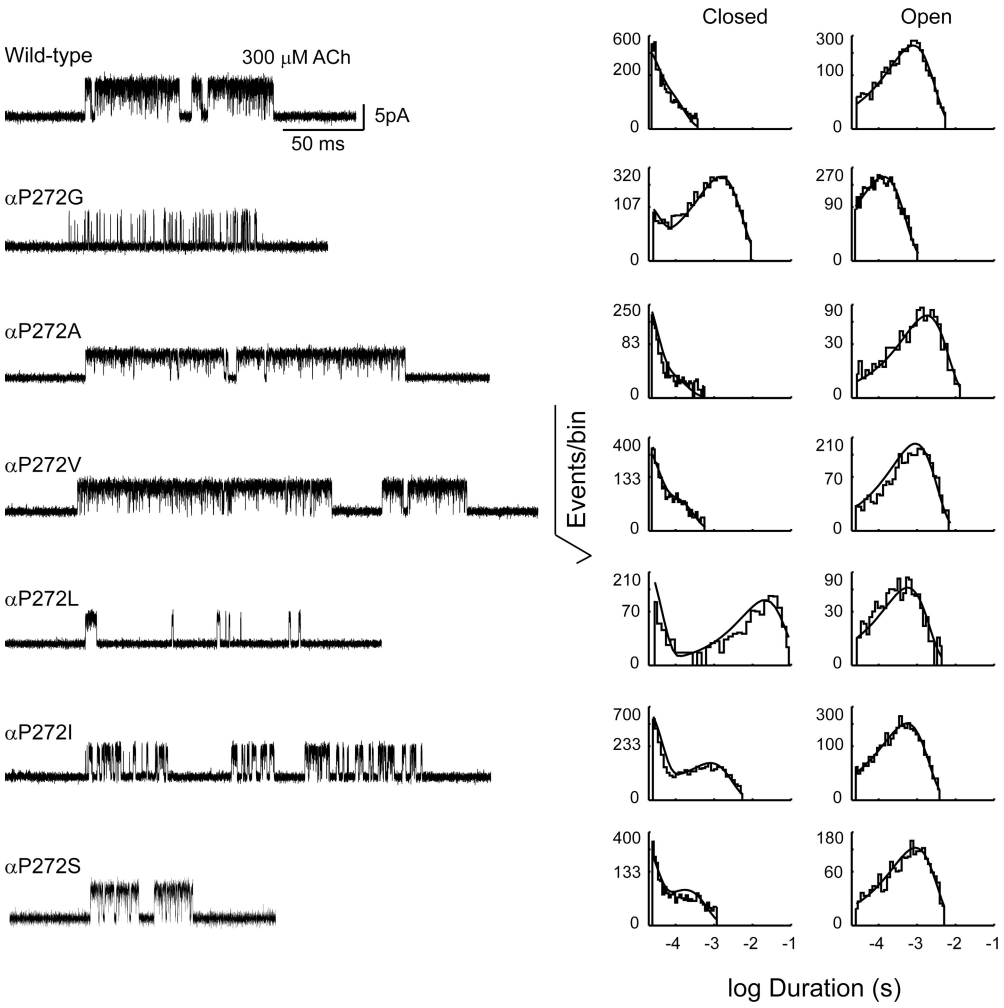

Figure 3. Single-channel currents and dwell time histograms from AChRs containing mutations of αPro 272. Currents elicited by 300 μM ACh are shown at a bandwidth of 10 kHz with channel openings upward deflections. Histograms of dwell times within identified clusters of events are shown on logarithmic time axes with probability density functions generated from global kinetic fitting overlaid (see Materials and methods; fitted rate constants are given in Tables I and II).

to the diverse range of channel gating kinetics among members of the Cys-loop receptor superfamily.

Contributions of Local Hydrophobic Residues to Channel Gating

αPro 272, αVal 132, and αVal 46 contribute to gating of the AChR channel (Chakrapani et al., 2003; Chakrapani and Auerbach, 2005; Lee and Sine, 2005), but the structural bases for their contributions remain to be elucidated. To investigate the structural nature of the contributions, we constructed a series of mutations of αPro 272, αVal 132, and αVal 46, transfected BOSC 23 cells with cDNAs encoding each mutant α-subunit, together with wild-type β, ε, and δ subunits, and recorded single-channel currents evoked by a wide range of ACh concentrations. Our initial studies centered on mutations of αPro 272, which is located in the middle of the M2–M3 loop and was suggested to trigger channel gating of the 5-HT_{3A} receptor channel through a trans-to-cis isomerization (Lummis et al., 2005). The recordings illustrated in Fig. 3 employed a saturating concentration of ACh in the patch pipette and allowed direct evaluation of the channel gating step based on the fraction of time the channel spent in the open versus the closed state. Whereas the wild-type AChR channel gates with high efficiency, substitutions of the large hydrophobic residues Ile and Leu, the small Gly, or the hydrophilic Ser impair channel gating (Fig. 3). Impaired gating produced by these substitutions is consistent with the trans-to-cis isomerization hypothesis, as they are not expected to allow significant formation of the cis isomer. By contrast, however, the Val substitution maintains rapid and efficient channel gating similar to the wild-type AChR, while the Ala substitution enhances gating. Like the first four substitutions, the Ala and Val substitutions are not expected to allow significant formation of the cis isomer; the efficient channel gating of AChRs harboring these substitutions indicates a different structural mechanism underlies gating of the muscle AChR. Instead, our findings suggest the residue at position α272 is chosen to achieve both steric and hydrophobic compatibility with the surrounding residues.

To quantify changes in channel gating of the mutant AChRs, we obtained recordings over a wide range of ACh concentrations and analyzed the resulting set of open and closed dwell times by fitting a kinetic scheme

TABLE I

Kinetic Analysis of Wild-Type and αP272 Mutant Receptors

Mutant	k_{+1}	k_{-1}	K_1	k_{+2}	k_{-2}	K_2	β_1	α_1	Θ_1	β_2	α_2	Θ_2	k_{+b}	k_{-b}	K_B	$\Delta G°$
			μM			*μM*									*mM*	*kcal/mol*
Wild type	271 ± 16	7190 ± 545	26	192 ± 6	19300 ± 309	101	67 ± 8	2190 ± 160	0.03 ± 0.0043	43700 ± 999	1650 ± 32	26.5 ± 0.79	26 ± 1	113000 ± 1690	4.3	–
αP272G	31 ± 19	895 ± 653	29	115 ± 26	13400 ± 2440	117	NA	NA	–	1260 ± 29	7410 ± 72	0.17 ± 0.004	17 ± 2	95800 ± 4920	5.6	2.96 ± 0.04
αP272A	48 ± 3	139 ± 14	2.9	84 ± 2	7100 ± 171	85	119 ± 9	475 ± 28	0.25 ± 0.024	40100 ± 1140	461 ± 12	87 ± 3.35	24 ± 1	130000 ± 1780	5.4	−0.70 ± 0.05
αP272V	168 ± 29	1620 ± 298	9.6	109 ± 4	24600 ± 615	226	NA	NA	–	32400 ± 1240	1010 ± 24	32 ± 1.45	22 ± 1	107000 ± 2200	4.9	−0.11 ± 0.06
αP272L	12 ± 8	228 ± 162	19	NA	NA	–	NA	NA	–	60.1 ± 1.9	1420 ± 26	0.042 ± 0.002	19 ± 2	110000 ± 4490	5.8	3.77 ± 0.05
αP272I	40 ± 12	478 ± 168	12	25 ± 1	8200 ± 363	328	18 ± 2	3850 ± 391	0.005 ± 0.0007	3410 ± 152	1030 ± 14	3.3 ± 0.15	31 ± 1	99400 ± 1710	3.2	1.22 ± 0.06
αP272S	153 ± 27	1120 ± 224	7.3	72 ± 2	18300 ± 500	254	69 ± 6	2450 ± 125	0.028 ± 0.0028	13200 ± 391	917 ± 12	14 ± 0.47	22 ± 1	120000 ± 1870	5.5	0.36 ± 0.04

Kinetic parameters and error estimates are derived from global fitting of kinetic scheme to data obtained over a wide range of ACh concentrations (Materials and methods). Units are $\mu M^{-1}s^{-1}$ for the association rate constants, s^{-1} for all others. Gating equilibrium constants (Θ) are ratios of channel opening (β) to closing rate (α) constants. NA, state is not included in the kinetic scheme. Free energy change ($\Delta G°$) = RTln(Θmutant/Θwild-type), where R is gas constant (1.987 cal/K·mol) and T is absolute temperature (295°K).

in which two ACh molecules bind to closed AChRs followed by channel opening and block of the open channel (see Materials and methods). For each type of AChR, long closed dwell times corresponding to sojourns in desensitized states were systematically removed as described previously (Lee and Sine, 2004; Mukhtasimova and Sine, 2007), and the resulting set of global dwell times was analyzed using a search algorithm that optimized the rate constants by maximizing the likelihood (Qin, et al., 1996). For receptors with or without substitutions of αPro 272, probability density functions generated from global fitting well describe the distributions of closed and open dwell times obtained over the entire range of ACh concentrations; only results obtained in the presence of the saturating concentration of 300 μM ACh are shown due to space limitations. The fitted rate

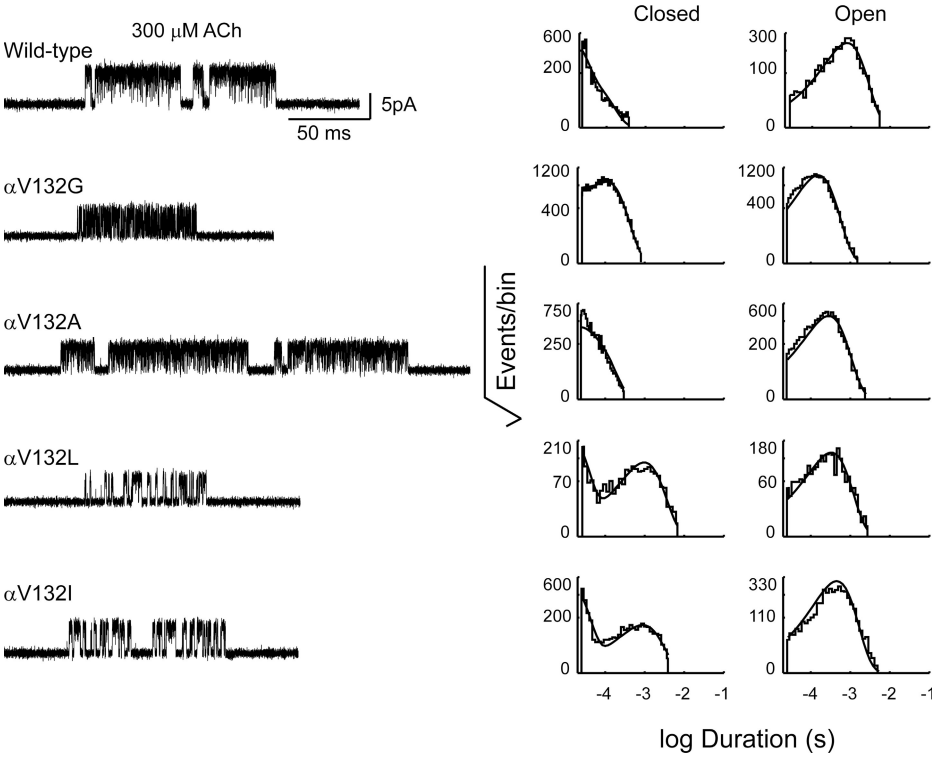

Figure 4. Single-channel currents and dwell time histograms from AChRs containing mutations of αVal 132. Currents elicited by 300 μM ACh are shown at a bandwidth of 10 kHz, with channel openings upward deflections. Histograms of dwell times within identified clusters of events are shown on logarithmic time axes with probability density functions generated from global kinetic fitting overlaid (see Materials and methods; fitted rate constants are given in Tables I and II).

TABLE II

Kinetic Analysis of Wild-Type, αV46, and αV132 Mutant Receptors

Mutant	k_{+1}	k_{-1}	K_1	k_{+2}	k_{-2}	K_2	β_1	α_1	Θ_1	β_2	α_2	Θ_2	k_{+b}	k_{-b}	K_B	$\Delta G°$
			μM			*μM*									*mM*	*kcal/mol*
Wild type	271 ± 16	7190 ± 545	26	192 ± 6	19300 ± 309	101	67 ± 8	2190 ± 160	0.03 ± 0.0043	43700 ± 999	1650 ± 32	26.5 ± 0.79	26 ± 1	113000 ± 1690	4.3	-
αE45A	296 ± 37	5300 ± 770	18	173 ± 6	19500 ± 447	113	NA	NA	-	28900 ± 504	13700 ± 153	2.1 ± 0.04	21 ± 1	110000[a]	5.2	1.48 ± 0.05
αV46G	NA	NA	-	NA	NA	-	NA	NA	-	115 ± 12	7870 ± 168	0.015 ± 0.002	40 ± 8	128000 ± 8670	3.2	4.40 ± 0.12
αV46A	111 ± 55	3100 ± 1560	28	55 ± 31	9490 ± 5130	173	51 ± 7	6560 ± 320	0.008 ± 0.001	155 ± 5	2740 ± 51	0.057 ± 0.002	26 ± 1	95500 ± 1990	3.7	3.60 ± 0.05
αV46L	328 ± 27	3140 ± 319	9.6	267 ± 11	7130 ± 144	27	NA	NA	-	40200 ± 636	4880 ± 81	8.2 ± 0.19	83 ± 8	120000 ± 4240	1.4	0.69 ± 0.05
αV46I	434 ± 39	4740 ± 486	11	217 ± 5	14300 ± 204	66	NA	NA	-	36500 ± 412	5360 ± 54	6.8 ± 0.10	17 ± 1	92900 ± 1960	5.5	0.80 ± 0.05
αV132G	718 ± 384	5180 ± 3000	7.2	222 ± 9	7860 ± 296	35	NA	NA	-	12900 ± 123	7830 ± 51	1.7 ± 0.02	19 ± 1	82600 ± 2110	4.4	1.63 ± 0.04
αV132A	324 ± 31	3040 ± 401	9.4	267 ± 11	10200 ± 255	38	77 ± 34	6840 ± 1030	0.011 ± 0.005	26600 ± 313	5430 ± 61	4.9 ± 0.08	18 ± 1	98700 ± 3130	5.5	0.99 ± 0.03
αV132L	97 ± 65	2030 ± 1430	21	107 ± 16	32300 ± 4510	302	NA	NA	-	2540 ± 91	2640 ± 30	0.96 ± 0.04	22 ± 1	99300 ± 2420	4.5	1.94 ± 0.06
αV132I	86 ± 44	3220 ± 1810	37	194 ± 69	40000 ± 13900	206	NA	NA	-	2280 ± 73	1580 ± 20	1.4 ± 0.05	24 ± 1	95700 ± 1910	4.0	1.71 ± 0.05

Kinetic parameters and error estimates are derived from global fitting of kinetic scheme to data obtained over a wide range of ACh concentrations (Materials and methods). Units are $\mu M^{-1}s^{-1}$ for the association rate constants, s^{-1} for all others. Gating equilibrium constants (Θ) are ratios of channel opening (β) to closing rate (α) constants. NA, state is not included in the kinetic scheme. Free energy change ($\Delta G°$) = RTln(Θmutant/Θwild-type), where R is gas constant (1.987 cal/K·mol) and T is absolute temperature (295°K).

[a]Value was constrained.

constants reveal that, compared with the wild-type AChR, substitutions of αPro 272 alter the channel gating equilibrium constant, while producing smaller changes in rate constants underlying ACh binding (Table I). Relative to the wild-type AChR, the free energy change of the channel gating step, ΔG^o, shows large positive values for

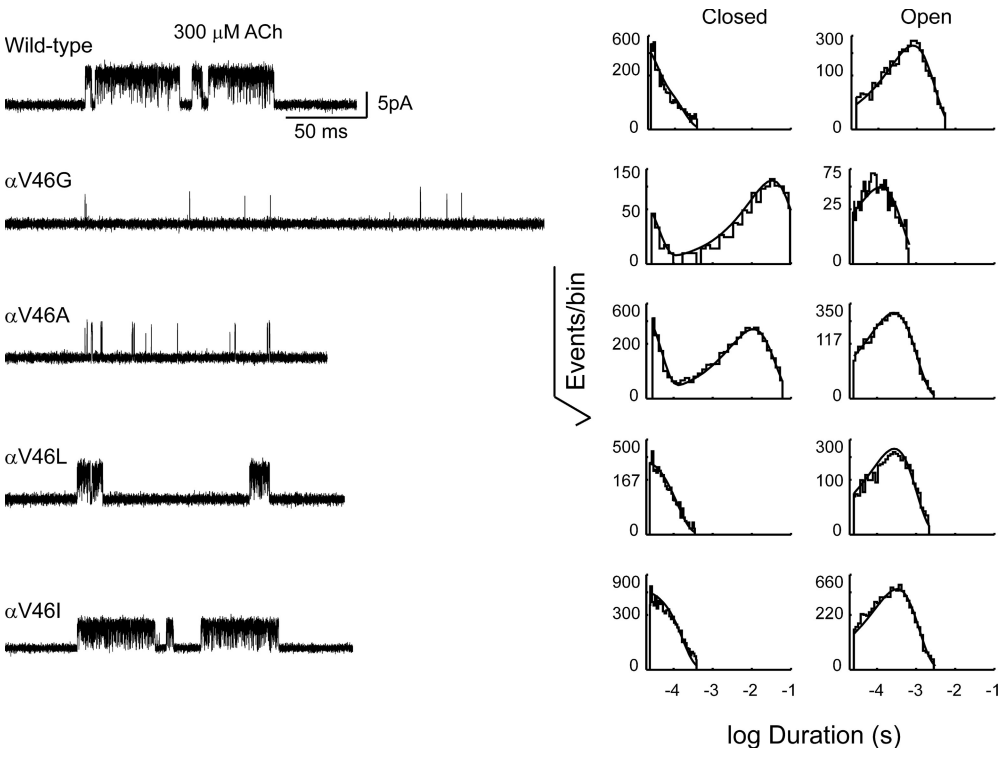

Figure 5. Single-channel currents and dwell time histograms from AChRs containing mutations of αVal 46. Currents elicited by 300 μM ACh are shown at a bandwidth of 10 kHz, with channel openings upward deflections. Histograms of dwell times within identified clusters of events are shown on logarithmic time axes with probability density functions generated from global kinetic fitting overlaid (see Materials and methods; fitted rate constants are given in Tables I and II).

the bulky hydrophobic and small Gly substitutions, a moderately negative value for the Ala substitution and small values for the Val and Ser substitutions. Thus, quantitative changes in rate and equilibrium constants for channel gating further suggest that Pro at position α272 enables rapid and efficient channel gating by providing the optimal size and hydrophobicity.

The structural model of the *Torpedo* AChR shows that αVal 132 and αVal 46 bracket αPro 272, suggesting the three residues form a pin-in-socket structure that joins the Cys, β1–β2, and M2–M3 loops. To test this possibility, we substituted each Val residue with a series of residues with different aliphatic side chains, from Gly to Leu, and recorded single-channel currents evoked by a range of ACh concentrations. Substitutions of αVal 132 prolong closed times and shorten open times (Fig. 4), decreasing the channel gating equilibrium constant (Table II). Kinetic analyses of the dwell times show that the small Gly and large Leu and Ile substitutions produce the greatest decreases in the channel gating equilibrium constant, while the Ala substitution produces a moderate decrease. Thus among residues with aliphatic side chains, Val at position α132 is optimal.

Substitutions of Val 46 also reduce the efficiency of channel gating, again by prolonging closed times and shortening open times (Fig. 5). Kinetic analyses of single-channel dwell times reveals that the small Gly and Ala substitutions profoundly decrease the gating equilibrium constant, up to 1,800-fold, while the larger Leu and Ile substitutions produce modest decreases (Table II). Thus similar to αVal 132, Val at position α46 is optimal.

For each of the three hydrophobic residues, αPro 272, αVal 132, and αVal 46, a plot of channel gating equilibrium constant against side chain volume shows a peak with the native side chain at or near the peak (Fig. 6). For αPro 272, a second peak is observed corresponding to the Ala substitution, which substantially enhances channel gating. From a structural viewpoint, the Ala substitution appears to provide the minimal size to form an anchor within the cavity created by the flanking Val residues. However, from a functional viewpoint, the resulting slow channel closing rate constant of 460 s^{-1} produced by the Ala substitution would prolong channel openings, reminiscent of slow channel myasthenic syndromes (Sine and Engel, 2006), and thus would be selected against. The findings thus far suggest the three juxtaposed residues are stabilized by their mutual hydrophobicity together with an optimized steric fit.

Energetic Coupling among αPro 272, αVal 132, and αVal 46

The structural continuity of these three hydrophobic residues and the functional consequences of single residue substitutions suggest the residues are interdependent in

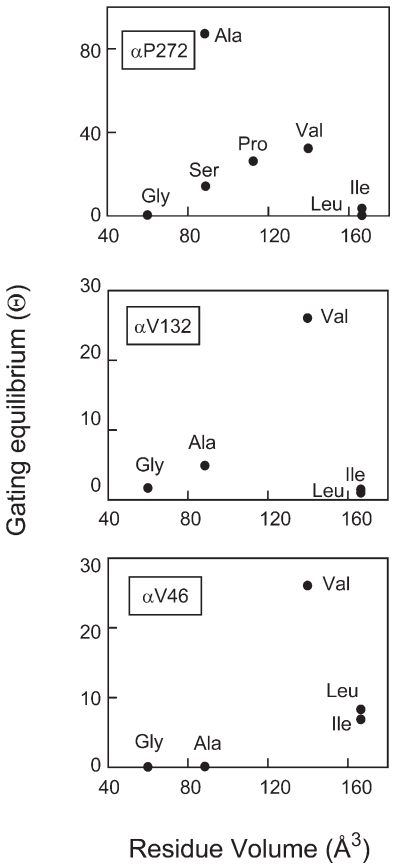

Figure 6. Dependence of the channel gating equilibrium constant on side chain volume of the residues substituted for αVal 46, αVal 132, and αPro 272. Channel gating equilibrium constants (Θ) are ratios of the rate constants for channel opening (β) and closing (α) determined by global kinetic fitting (see Materials and methods and Tables I and II).

contributing to channel gating. To determine whether the functional contributions are interdependent, we generated individual AChRs containing from one to three Ala substitutions at the three positions, determined channel gating equilibrium constants (Θ_2) for each mutant AChR, and cast the results as cubic mutant cycles.

We first consider how the contribution of αPro 272 to channel gating depends on αVal 46, without and with substitution of αVal 132 (Fig. 7 A, top and bottom planes). The mutation αP272A increases the channel gating equilibrium constant threefold and αV46A decreases it 470-fold, but the combined mutations produce only a 1.7-fold decrease (Tables I–III). The resulting inter-residue coupling free energy is large, −2.6 kcal/mol (Fig. 7 A, top plane); coupling free energy is negative because channel gating is enhanced relative to that expected from independent contributions of the two individual mutations. A possible structural explanation of the negative coupling energy is the αP272A mutation establishes a productive interaction with a surrounding residue or residues that more than compensates for the suppression of gating by αV46A.

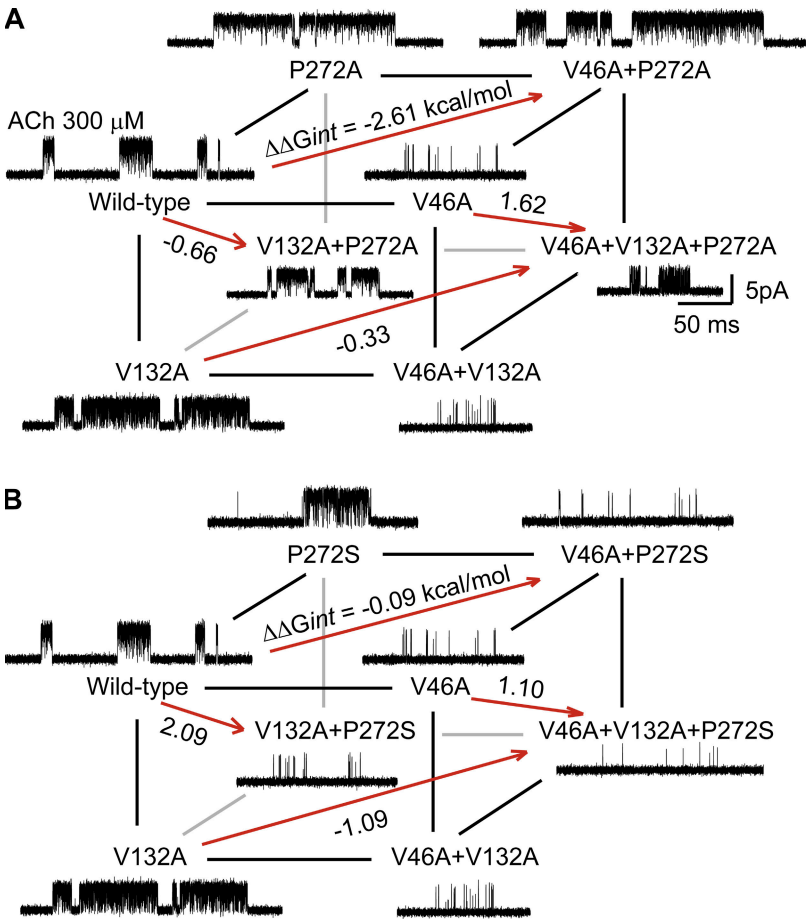

Figure 7. Energetic coupling between residues αVal 46, αPro 272, and αVal 132. Each plane of the cubic mutant cycle depicts coupling and the corresponding free energies ($\Delta\Delta G_{int}$) for a specified residue pair; one plane represents coupling in the wild-type AChR background, whereas the parallel plane represents coupling in a mutant AChR background. For each mutant AChR, single-channel currents elicited by 300 μM ACh are shown at a bandwidth of 10 kHz. (A) Cubic mutant cycle in which Ala is substituted for αPro 272. For the front plane, $\Delta\Delta G_{int} = -1.1$ kcal/mol, and for the back plane $\Delta\Delta G_{int} = 1.2$ kcal/mol. (B) Cubic mutant cycle in which Ser is substituted for αPro 272. For the front plane, $\Delta\Delta G_{int} = -1.1$ kcal/mol, and for the back plane $\Delta\Delta G_{int} = -2.05$ kcal/mol.

On the other hand, when the mutation αV132A is present in the same AChR, the αP272A/αV46A mutant cycle yields a coupling free energy of only −0.33 kcal/mol (Fig. 7 A, bottom plane). A possible structural explanation is the productive interaction that enables efficient gating of the αP272A mutant requires αVal132, and substitution of Ala for αVal 132 removes that productive interaction. Thus the strong coupling between αPro 272 and αVal 46 depends upon αVal 132.

Conversely, we asked how the contribution of αPro 272 depends on αVal 132, without and with substitution of αVal 46 (Fig. 7 A, left and right planes). In the wild-type AChR background, the mutant cycle αP272A/αV132A shows a coupling free energy of −0.66 kcal/mol. However when the mutation αV46A is present in the same AChR, coupling free energy increases to 1.6 kcal/mol; coupling free energy is positive because channel gating is suppressed relative to that expected from independent contributions of the two individual mutations. The interplane difference in coupling free energy is large, 2.3 kcal/mol, indicating that αPro 272 energetically couples to αVal 132, and that this coupling depends upon αVal 46; thus the three residues form a functionally interdependent triad.

To further test the interdependence of the residue triad, we asked whether the functional contribution of αVal 132 depends on αVal 46, without and with substitution of αPro 272 (Fig. 7 A, front and back planes). In the wild-type AChR background, the αV132A/αV46A mutant cycle shows a moderate coupling free energy of −1.1 kcal/mol, but when the mutation αP272A is present in the same AChR, coupling free energy increases to 1.2 kcal/mol (Table III). The interplane difference in coupling free energy is large, 2.3 kcal/mol; thus although αVal 132 and αVal 46 do not make direct contact, they are functionally coupled through αPro 272.

Dependence of Inter-residue Energetic Coupling on the Substituting Residue

The preceding findings show that energetic coupling among any pair of residues of the triad depends on the third residue, suggesting the overall structure of the triad ultimately determines the channel gating equilibrium constant. Furthermore when Ala is substituted for αPro 272, the rate constant for channel opening (β_2) increases, and the brief closed time component associated with channel opening approaches the resolution limit of the recording system (Fig. 3), potentially causing an underestimate of the channel gating equilibrium constant. Thus to address both the structural dependence of inter-residue coupling and the potential

TABLE III

Energetic Coupling of αE45, αV46, αV132, and αP272

Receptors	β	α	Θ	$\Delta\Delta G_{int}$	$\Delta\Delta\Delta G_{int}$
	s^{-1}	s^{-1}	β/α	*kcal/mol*	*kcal/mol*
V132A-P272A	71800 ± 1680	1440 ± 47	50 ± 2.0	−0.66 ± 0.07	
V132L-P272A	16700 ± 517	1290 ± 18	13 ± 0.44	−0.83 ± 0.07	
V132A-P272L	186 ± 5.4	1010 ± 17	0.18 ± 0.006	−1.85 ± 0.06	
V132L-P272L	62 ± 3.1	3240 ± 78	0.019 ± 0.001	−1.48 ± 0.08	
V132A-P272S	522 ± 12	6980 ± 91	0.075 ± 0.002	2.09 ± 0.05	
V46A-P272A	40900 ± 1150	2550 ± 50	16 ± 0.55	−2.61 ± 0.07	
V46A-P272L	NA	NA	-	-	
V46A-P272S	64 ± 2.1	1780 ± 32	0.036 ± 0.001	−0.094 ± 0.07	
V46A-V132A	797 ± 14	12700 ± 150	0.081 ± 0.002	−1.05 ± 0.07	
V46A-V132L	NA	NA	-	-	
E45A-V46A	78 ± 1.3	16800 ± 240	0.0046 ± 0.0001	−0.018 ± 0.057	
E45A-V132A	14000 ± 109	17000 ± 108	0.82 ± 0.0082	−0.44 ± 0.04	
E45A-P272A	83900 ± 1610	2150 ± 66	39 ± 1.4	−1.01 ± 0.06	
E45A-P272S	11400 ± 182	6370 ± 59	1.79 ± 0.03	−0.26 ± 0.05	
V46A-P272A-V132A	7210 ± 77	6420 ± 48	1.12 ± 0.015		2.28 ± 0.05
V46A-P272S-V132A	80 ± 2.7	13000 ± 380	0.0062 ± 0.0003		−1.00 ± 0.07
E45A-P272A-V132A	45300 ± 346	6330 ± 61	7.2 ± 0.089		1.10 ± 0.04
E45A-P272S-V132A	2870 ± 486	29900 ± 646	0.096 ± 0.016		−0.93 ± 0.18

Kinetic parameters and error estimates are derived from global fitting of kinetic scheme to data obtained over a wide range of ACh concentrations (Materials and methods). Gating equilibrium constant (Θ) is ratio of channel opening (β) to closing rate (α) constants. NA, channel openings were detected but clear clusters of openings did not form, preventing kinetic analyses.

technical limitation, we asked whether inter-residue energetic coupling depends on the choice of the residue substituted for the central αPro 272.

We chose Ser as the alternative substitution for αPro 272 because it results in a hydrophilic residue between the flanking Val residues, and αP272S slows rather than speeds the rate constant for channel opening (Table I). The mutant cycle αP272S/αV46A yields a coupling free energy of −0.09 kcal/mol (Fig. 7 B, top plane; Table III), in contrast to the coupling energy of −2.6 kcal/mol obtained for the mutant cycle αP272A/αV46A (Fig. 7 A, top plane). However when the mutation αV132A is present in the same AChR, the αP272S/αV46A mutant cycle yields a coupling free energy of −1.1 kcal/mol. Thus the magnitude of the coupling free energy between αPro 272 and αVal 46 depends on whether Ala or Ser is substituted for αPro 272, as well as on whether αV132 is substituted with Ala.

On the other hand, the mutant cycle αP272S/αV132A yields a coupling free energy of 2.1 kcal/mol (Fig. 7 B, left plane; Table III), in contrast to the mutant cycle αP272A/αV132A, which yielded a coupling energy of −0.66 kcal/mol (Fig. 7 A, left plane). When the mutation αV46A is present in the same AChR, coupling energy for the αP272S/αV132A decreases to 1.1 kcal/mol (Fig. 7 B, right plane). Thus coupling between αPro 272 and αVal 132 also depends on whether Ala or Ser is substituted for αPro 272, as well as on whether αVal 46 is substituted with Ala. The overall findings suggest that the large pairwise coupling energies inherent to the residue triad can be shifted from one pair of residues to another by changing the substitution of the central αPro 272 from Ala to Ser.

The mutant cycle comprising αV46A and αV132A yielded coupling free energies of −1.1 and 1.2 kcal/mole in wild-type and αP272A backgrounds, respectively (Fig. 7 A, front and back planes), yielding an interplane difference of 2.3 kcal/mol. However, when Ser rather than Ala is substituted for αPro 272, the αV46A/αV132A cycle yields a coupling free energy of −2.1 kcal/mol (Fig. 7 B, back plane), giving an interplane difference of −1.0 kcal/mol. This smaller interplane difference shows that αV46A and αV132A are more strongly interdependent when αPro 272 contains a hydrophobic rather than a hydrophilic substitution, further supporting a role for hydrophobicity in stabilizing the residue triad.

Energetic Coupling among αGlu 45, αPro 272, and αVal 132

In the *Torpedo* AChR structural model, αGlu 45 projects from the β1–β2 loop toward αArg 209, with the aliphatic portion of the Glu side chain approaching αPro 272 as it crosses the M2–M3 linker. We previously demonstrated inter-residue energetic coupling between αGlu 45 and αPro 272, and showed that this coupling depended on substitution of αVal 46 (Lee and Sine, 2005). In light of the present findings, we asked whether coupling between αGlu 45 and αPro 272 depends on αVal 132. The mutant cycle αE45A/αP272A yields an inter-residue coupling free energy of −1.0 kcal/mol (Fig. 8 A, left

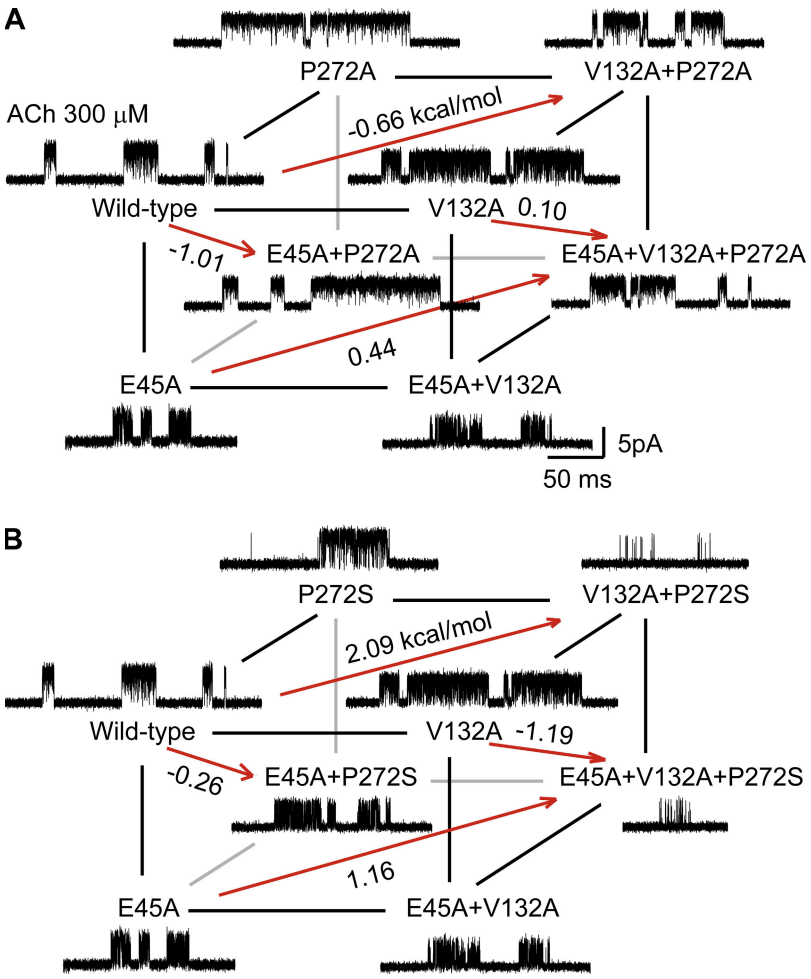

Figure 8. Energetic coupling between residues αVal 132, αPro 272, and αGlu 45. Each plane of the cubic mutant cycle depicts coupling and the corresponding free energies ($\Delta\Delta G_{int}$) for a specified residue pair; one plane represents coupling in the wild-type AChR background, whereas the parallel plane represents coupling in a mutant AChR background. For each mutant AChR, single-channel currents elicited by 300 μM ACh are shown at a bandwidth of 10 kHz. (A) Cubic mutant cycle in which Ala is substituted for αPro 272. For the front plane, $\Delta\Delta G_{int}$ = −0.44 kcal/mol, and for the back plane $\Delta\Delta G_{int}$ = 0.67 kcal/mol. (B) Cubic mutant cycle in which Ser is substituted for αPro 272. For the front plane, $\Delta\Delta G_{int}$ = −0.44 kcal/mol, and for the back plane $\Delta\Delta G_{int}$ = −1.4 kcal/mol.

plane), but when the mutation αV132A is present in the same AChR, the coupling energy decreases to 0.1 kcal/mol (Fig. 8 A, right plane), giving an interplane difference of 1.1 kcal/mol. The analogous mutant cycle αE45A/αP272S yields a coupling free energy of −0.26 kcal/mol, but when the mutation αV132A is present in the same AChR, coupling free energy increases to −1.2 kcal/mol, giving an interplane difference of −0.9 kcal/mol (Fig. 8 B, left and right planes). Thus, coupling between αGlu 45 and αPro 272 depends on αVal 132, and the coupling energy can shift from one vertical plane to another depending on whether Ala or Ser is substituted for αPro 272.

Conversely, we asked whether the contribution of αGlu 45 depends on αVal 132 in receptors without and with the mutations αP272A or αP272S. In the wild-type AChR background, the mutant cycle αE45A/αV132A yields an inter-residue coupling free energy of −0.44 kcal/mol (Fig. 8 A, front plane), but when the mutation αP272A is present in the same AChR, coupling free energy increases to 0.67 kcal/mol (Fig. 8 A, back plane), giving an interplane difference of 1.1 kcal/mol. On the other hand, when the mutation αP272S is present in the same AChR, the αE45A/αV132A cycle yields a coupling free energy of −1.4 kcal/mol (Fig. 8 B, back plane), giving an interplane difference of −0.9 kcal/mol. Thus, although the αGlu 45 and αVal 132 side chains do not make direct contact, the two residues are energetically coupled through the intervening αPro 272. αGlu 45, αPro 272, and αVal 132 constitute a second triad with moderate inter-residue coupling energies, which again can shift from residue pair to another depending on whether Ala or Ser is substituted for αPro 272.

DISCUSSION

The present findings contribute to the developing picture of how binding of ACh triggers gating of the remote AChR channel. The triggering process begins when ACh binds within the aromatic-rich binding pocket and the C-loop at the periphery of the pocket changes from an uncapped to a capped conformation, trapping ACh (Gao et al., 2005, 2006; Hansen et al., 2005; Law et al., 2005). The uncapped conformation is stabilized by a salt bridge between αAsp 200 of β-strand 10 and αLys 145 of β-strand 7 (Celie, et al., 2004). However, when the capped conformation forms, an additional salt bridge is established between αTyr 190 of the C-loop and αLys 145

(Celie et al., 2004), which was shown to be a decisive early step in the agonist binding to channel gating transduction process (Mukhtasimova et al., 2005). Both β strands 7 and 10 extend from the ligand binding site to the interface of the binding and pore domains and thus are positioned to transmit structural changes over the long distance to the pore. At the junction of the ligand binding and pore domains, a conserved salt bridge between αArg 209 of β-strand 10 and αGlu 45 of the β1–β2 loop positions αVal 46 of the β1–β2 loop between αPro 272 and αSer 269 of the M2–M3 linker (Unwin, 2005; Fig. 1), forming a pin-in-socket assembly that functionally links the two domains (Lee and Sine, 2005). The current findings provide evidence for a second, functionally crucial pin-in-socket assembly adjacent to the first, comprising the hydrophobic side chains of αVal 132, αPro 272, and αVal 46.

The cryoelectron microscopic structural model of the *Torpedo* AChR provided the first structural evidence of a pin-in-socket assembly composed of αVal 46 as the pin and αSer 269 and αPro 272 as the socket (Miyazawa, et al., 2003; Unwin, 2005). All three of these residues are essential for rapid and efficient channel gating (Chakrapani, et al., 2004; Lee and Sine, 2005; Jha, et al., 2007), and are energetically coupled (Lee and Sine, 2005), providing support for the *Torpedo* AChR structural model. Although none of the three residues is conserved, an inter-residue interaction based on hydrophobicity and steric fit is likely. Among members of the Cys-loop receptor superfamily, side chains of the three residues contain a range of hydrophilic and hydrophobic elements, suggesting naturally occurring substitutions may alter the balance of elements to produce a wide range of channel gating rate and equilibrium constants. For example at position α269, the naturally occurring Ser may achieve the correct hydrophobic-to-hydrophilic balance to optimize the interaction strength with αVal 46 and αPro 272. The mutation αS269L increases hydrophobicity and enhances channel gating (Lee and Sine, 2005), possibly because the substituted Leu increases hydrophobic stabilization with αVal 46 and αPro 272. Such an enhanced interaction would be undesirable for the muscle AChR, however, as it would significantly prolong the synaptic response. The present study provides evidence for a second pin-in-socket structure comprising αPro 272 as the pin and αVal 46 and αVal 132 as the socket. We find that the functional contributions of these residues depend jointly on proper steric fit and hydrophobicity, and the residues show strong pairwise energetic coupling, providing support for the residue locations in the *Torpedo* AChR structural model. Thus two contiguous pin-in-socket structures join the β1–β2 and Cys loops from the binding domain with the M2–M3 linker from the pore domain.

Double mutant cycle analyses have been widely employed to assess inter-residue interactions within proteins (Horovitz and Fersht, 1990; Horovitz, et al., 1990). The analysis is based on the principle that the free energy change due to mutation of a single residue, ΔG_1, depends on other residues within the protein. If mutation of a second residue affects the free energy change caused by mutation of the first residue, giving ΔG_2, the two residues interact with a first order coupling free energy, $\Delta\Delta G = \Delta G_2 - \Delta G_1$. A negative value of $\Delta\Delta G$ indicates the free energy change of the double mutant is more favorable than expected from the sum of free energy changes of the single mutants, whereas a positive value indicates the free energy change of the double mutant is less favorable than expected from the sum of free energy changes of the single mutants. Inter-residue coupling free energy is a thermodynamic parameter and does not specify whether the coupling arises through a direct or a propagated interaction. However if the 3D structure is known, and the two residues are juxtaposed, the simplest interpretation is that in the context of the surrounding structure, the coupling arises through direct contact.

In the present study, αPro 272 and αVal 46 emerge as the most strongly coupled residue pair. In the wild-type AChR background, the mutation αP272A enhances channel gating ($\Delta G_1 = -0.7$ kcal/mol), but in the presence of the mutation αV46A, gating is enhanced much more strongly ($\Delta G_2 = -3.3$ kcal/mol), yielding a first order coupling free energy of −2.6 kcal/mol. Because αPro 272 and αVal 46 are proximal in the *Torpedo* AChR structural model, direct interaction is likely. However after substituting the flanking αVal 132 with Ala, coupling between αPro 272 and αVal 46 decreases to −0.3 kcal/mol, indicating that the strong pairwise coupling is context dependent. Within the αP272A/αV132A/αV46A cubic mutant cycle, the difference between the two parallel αP272A/αV46A mutant cycles gives a second order coupling energy $\Delta\Delta G_2 - \Delta\Delta G_1$ of 2.3 kcal/mol. Context dependence of inter-residue coupling has been widely observed in proteins and was illustrated by a classical example in which Ala was substituted for three charged and two polar residues in the complex formed by TEM-β-lactamase and its protein inhibitor BLIP (Albeck, et al., 2000). When either of the two salt bridges was installed alone into the Ala background, the charge–charge interaction was neutral or repulsive, but in the native structure the salt bridges were strongly stabilizing.

Perhaps unexpectedly, when Ser is substituted for αPro 272, coupling energy for the αP272S/V46A mutant cycle is negligible ($\Delta\Delta G = -0.1$ kcal/mol), indicating the two residues lost their mutual dependence. The likely reason is that, owing to the dynamic nature of protein structure, introduction of a hydrophilic residue within the local hydrophobic network shifted the inter-residue interaction from one residue pair to another. Evidence for a shift of the interaction comes from the observation that whereas the αP272A/αV132A mutant cycle exhibits a low coupling

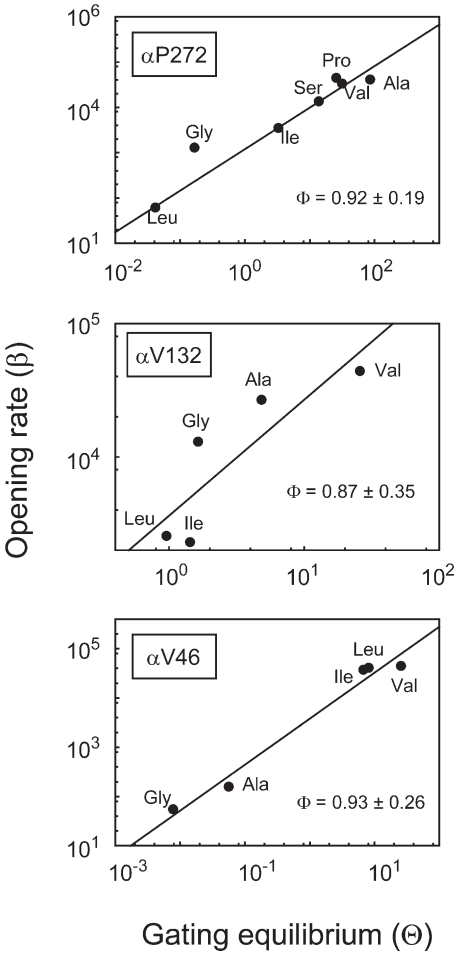

Figure 9. REFER analysis of mutations of αPro 272, αVal 132, and αVal 46. Channel opening rate constant is plotted against the channel gating equilibrium constant for the indicated substitutions of each residue. The values plotted are given in Tables I and II. Linear regression yielded the lines shown with the indicated slopes Φ and standard deviations.

free energy of −0.7 kcal/mol, the αP272S/αV132A mutant cycle exhibits a large coupling energy of 2.1 kcal/mol. Transfer of coupling energy among residue pairs may occur through local changes in polarity or charge (Sohn and Rudolph, 2006), changes in side chain volume within the confined protein interior (Schreiber and Fersht, 1995; Zhang, et al., 1996; Jain and Ranganathan, 2004), or from changes in residue contact with solvent (Covell and Wallqvist, 1997; Vaughan, et al., 1999). Nevertheless in AChRs containing the mutation αP272S, coupling with αVal 46 is evident from the second order coupling free energy of −1 kcal/mol obtained from the difference in first order coupling energies between the two parallel αP272S/αV132A mutant cycles. The overall findings show that αPro 272, αVal 132, and αVal 46 contribute to channel gating in an interdependent manner.

For most residues we have examined that contribute to channel gating, if the side chains are proximal in the *Torpedo* AChR structural model, energetic coupling is observed, whereas if the side chains are spatially separate and without an intervening residue, coupling is low or negligible. For example, αGlu 45 and αVal 46 are consecutive in the primary sequence, but show negligible coupling (Lee and Sine, 2005), likely because their side chains project in opposite directions. Similarly, αGlu 45 and αSer 269 are spatially separate and show low coupling. These observations agree with studies of the Barnase-Barstar interface, which showed that residues separated by <7 Å showed energetic coupling, whereas residues with larger separations showed independent contributions (Schreiber and Fersht, 1995).

A key question is what happens to the interloop triad when the channel switches from closed to open. A previous study of 5-HT_{3A} receptors suggested channel opening resulted from isomerization of αPro 272 from trans to cis (Lummis, et al., 2005). Although our substitutions of αPro 272 with natural amino acids may have altered the main chain structure of the M2–M3 loop, the observations of rapid and efficient channel gating with Ala and Val substitutions, which are expected to oppose formation of the cis isomer, show that the cis–trans isomerization mechanism does not apply to the muscle AChR.

The timing of structural changes in the binding-gating transduction process has been inferred from rate-equilibrium free energy relationships (REFER) in which the channel opening rate constant is plotted against the channel gating equilibrium constant for a series of substitutions of a given residue. In many instances a log–log plot of these quantities is linear, and the slope (Φ) is interpreted as an index of the open- versus closed-state conformation of the specified residues in the gating transition state (Auerbach, 2007). Values of Φ approaching 1 suggest the conformation of the transition state is open-like, whereas values approaching 0 suggest the conformation of the transition state is closed-like. Our data for human muscle AChRs activated by ACh show Φ values for substitutions of αPro 272, αVal 46, and αVal 132, ranging from 0.87 to 0.93 (Fig. 9). If Φ reflects the relative time at which the transition state is achieved, the similar Φ values suggest the three residues move nearly simultaneously as they approach an open-like transition state. Thus, if the *Torpedo* AChR structural model accurately depicts the interloop triad in the resting closed state, our findings indicate that the three residues maintain physical continuity up to the transition state. This conclusion is tentative because although our REFER plots for αP272 and αVal 46 are linear, the plot for αVal 132 is curved. On the other hand, REFER analyses of mouse muscle AChRs activated by either ACh or choline appeared linear and yielded statistically different values (αPro 272 [Φ = 0.62], αVal 46 [Φ = 0.81], and αVal 132 [Φ = 0.75]), suggesting somewhat asynchronous movement of the three residues (Chakrapani, et al., 2004; Jha, et al., 2007).

A key remaining question is whether the binding and pore domains remain physically engaged in the open state. Among possible physical mechanisms, the binding domain may be envisioned as a brake that maintains the pore in the closed state, but to allow channel opening, the binding domain disengages from the pore domain (Cheng et al., 2006). Normal mode analyses (NMA) of homology models of the α7 AChR reveal a major mode in which all the subunits undergo a quaternary twist about their long axes (Cheng et al., 2006; Taly et al., 2006). Furthermore, both NMA and all-atom molecular dynamics simulations found that motions of the β1–β2, Cys, and M2–M3 loops were correlated (Cheng et al., 2006, 2007), suggesting the triad maintains physical continuity in both the resting and open states. Although vibrational modes generated from NMA originate from the overall flexibility of the protein backbone, rather than from inter-side chain interactions, mutations could nevertheless alter the ability of juxtaposed loops to articulate freely and, in turn, alter rate and equilibrium constants underlying channel gating. Furthermore, if the binding and pore domains disengaged in the open state, substitutions of the smaller Ala for the three residues would be expected to promote disengagement and enhance gating. However, our AChR with the triple Ala substitution strongly suppresses channel gating, suggesting physical continuity of the binding and pore domains is maintained in the open state.

Studies of chimeric receptors showed that communication between the agonist binding site and the channel required structural compatibility among multiple loops within the structural transition zone between the binding and pore domains (Bouzat, et al., 2004). Beyond the present triad of β1–β2, Cys, and M2–M3 loops, additional functionally crucial inter-residue interactions likely remain to be elucidated. The Cys loop makes further contacts within the binding-pore transition zone, and additional contributing structures include the pre-M1 region of β-strand 10, the N terminus of M1, the β8–β9 loop, and the C terminus of M4. Furthermore, inter-residue contacts spanning subunit interfaces are required to enable rapid and efficient channel gating (Mukhtasimova and Sine, 2007). The vast array of structural, functional, and computational approaches now available offer powerful means to unmask the full set of intraprotein coupling structures, as well as disclose the symphony of coordinated motions that enable the remarkably rapid and efficient chemical to electrical transduction by the AChR.

We thank Kara Barber for contributions in the initial development of this work.

This work was supported by National Institutes of Health grant R37 NS31744 to S.M. Sine.

Olaf S. Andersen served as editor.

Submitted: 3 April 2008
Accepted: 10 July 2008

REFERENCES

Albeck, S., R. Unger, and G. Schreiber. 2000. Evaluation of direct and cooperative contributions towards the strength of buried hydrogen bonds and salt bridges. *J. Mol. Biol.* 298:503–520.

Auerbach, A. 2007. How to turn the reaction coordinate into time. *J. Gen. Physiol.* 130:543–546.

Bouzat, C., F. Gumilar, G. Spitzmaul, H.L. Wang, D. Rayes, S.B. Hansen, P. Taylor, and S.M. Sine. 2004. Coupling of agonist binding to channel gating in an ACh-binding protein linked to an ion channel. *Nature.* 430:896–900.

Brejc, K., W.J. van Dijk, R.V. Klaassen, M. Schuurmans, J. van Der Oost, A.B. Smit, and T.K. Sixma. 2001. Crystal structure of an ACh-binding protein reveals the ligand-binding domain of nicotinic receptors. *Nature.* 411:269–276.

Carter, P.J., G. Winter, A.J. Wilkinson, and A.R. Fersht. 1984. The use of double mutants to detect structural changes in the active site of the tyrosyl-tRNA synthetase (*Bacillus stearothermophilus*). *Cell.* 38:835–840.

Celie, P.H., S.E. van Rossum-Fikkert, W.J. van Dijk, K. Brejc, A.B. Smit, and T.K. Sixma. 2004. Nicotine and carbamylcholine binding to nicotinic acetylcholine receptors as studied in AChBP crystal structures. *Neuron.* 41:907–914.

Chakrapani, S., and A. Auerbach. 2005. A speed limit for conformational change of an allosteric membrane protein. *Proc. Natl. Acad. Sci. USA.* 102:87–92.

Chakrapani, S., T.D. Bailey, and A. Auerbach. 2003. The role of loop 5 in acetylcholine receptor channel gating. *J. Gen. Physiol.* 122:521–539.

Chakrapani, S., T.D. Bailey, and A. Auerbach. 2004. Gating dynamics of the acetylcholine receptor extracellular domain. *J. Gen. Physiol.* 123:341–356.

Cheng, X., H. Wang, B. Grant, S.M. Sine, and J.A. McCammon. 2006. Targeted molecular dynamics study of C-loop closure and channel gating in nicotinic receptors. *PLoS Comput. Biol.* 2:e134.

Cheng, X., I. Ivanov, H. Wang, S.M. Sine, and J.A. McCammon. 2007. Nanosecond-timescale conformational dynamics of the human α7 nicotinic acetylcholine receptor. *Biophys. J.* 93:2622–2634.

Colquhoun, D., and F. Sigworth. 1983. Fitting and statistical analysis of single channel records. *In* Single Channel Recording. B. Sakmann, and E. Neher, editors. Plenum Publishing Corp., New York. 191–264.

Covell, D.G., and A. Wallqvist. 1997. Analysis of protein-protein interactions and the effects of amino acid mutations on their energetics. The importance of water molecules in the binding epitope. *J. Mol. Biol.* 269:281–297.

Gao, F., N. Bren, T.P. Burghardt, S. Hansen, R.H. Henchman, P. Taylor, J.A. McCammon, and S.M. Sine. 2005. Agonist-mediated conformational changes in acetylcholine-binding protein revealed by simulation and intrinsic tryptophan fluorescence. *J. Biol. Chem.* 280:8443–8451.

Gao, F., G. Mer, M. Tonelli, S.B. Hansen, T.P. Burghardt, P. Taylor, and S.M. Sine. 2006. Solution NMR of acetylcholine binding protein reveals agonist-mediated conformational change of the C-loop. *Mol. Pharm.* 70:1230–1235.

Grutter, T., L.P. de Carvalho, V. Dufresne, A. Taly, S.J. Edelstein, and J.P. Changeux. 2005. Molecular tuning of fast gating in pentameric ligand-gated ion channels. *Proc. Natl. Acad. Sci. USA.* 102:18207–18212.

Hansen, S.B., G. Sulzenbacher, T. Huxford, P. Marchot, P. Taylor, and Y. Bourne. 2005. Structures of Aplysia AChBP complexes with nicotinic agonists and antagonists reveal distinctive binding interfaces and conformations. *EMBO J.* 24:3635–3646.

Hidalgo, P., and R. MacKinnon. 1995. Revealing the architecture of a K^+ channel pore through mutant cycles with a peptide inhibitor. *Science.* 268:307–310.

Horovitz, A., and A.R. Fersht. 1990. Strategy for analysing the co-operativity of intramolecular interactions in peptides and proteins. *J. Mol. Biol.* 214:613–617.

Horovitz, A., L. Serrano, B. Avron, M. Bycroft, and A.R. Fersht. 1990. Strength and co-operativity of contributions of surface salt bridges to protein stability. *J. Mol. Biol.* 216:1031–1044.

Jain, R.K., and R. Ranganathan. 2004. Local complexity of amino acid interactions in a protein core. *Proc. Natl. Acad. Sci. USA.* 101:111–116.

Jha, A., D.J. Cadugan, P. Purohit, and A. Auerbach. 2007. Acetylcholine receptor gating at extracellular transmembrane domain interface: the cys-loop and m2 m3 linker. *J. Gen. Physiol.* 130:547–558.

Kellis, J.T. Jr., K. Nyberg, D. Sali, and A.R. Fersht. 1988. Contribution of hydrophobic interactions to protein stability. *Nature.* 333:784–786.

Law, R.J., R.H. Henchman, and J.A. McCammon. 2005. A gating mechanism proposed from a simulation of a human α7 nicotinic acetylcholine receptor. *Proc. Natl. Acad. Sci. USA.* 102:6813–6818.

Lee, B.S., R.B. Gunn, and R.R. Kopito. 1991. Functional differences among nonerythroid anion exchangers expressed in a transfected human cell line. *J. Biol. Chem.* 266:11448–11454.

Lee, W.Y., and S.M. Sine. 2004. Invariant aspartic acid in muscle nicotinic receptor contributes selectively to the kinetics of agonist binding. *J. Gen. Physiol.* 124:555–567.

Lee, W.Y., and S.M. Sine. 2005. Principal pathway coupling agonist binding to channel gating in nicotinic receptors. *Nature.* 438:243–247.

Lummis, S.C., D.L. Beene, L.W. Lee, H.A. Lester, R.W. Broadhurst, and D.A. Dougherty. 2005. Cis-trans isomerization at a proline opens the pore of a neurotransmitter-gated ion channel. *Nature.* 438:248–252.

Miyazawa, A., Y. Fujiyoshi, and N. Unwin. 2003. Structure and gating mechanism of the acetylcholine receptor pore. *Nature.* 423:949–955.

Mukhtasimova, N., and S.M. Sine. 2007. An intersubunit trigger of channel gating in the muscle nicotinic receptor. *J. Neurosci.* 27:4110–4119.

Mukhtasimova, N., C. Free, and S.M. Sine. 2005. Initial coupling of binding to gating mediated by conserved residues in the muscle nicotinic receptor. *J. Gen. Physiol.* 126:23–39.

Ohno, K., H.L. Wang, M. Milone, N. Bren, J.M. Brengman, S. Nakano, P. Quiram, J.N. Pruitt, S.M. Sine, and A.G. Engel. 1996. Congenital myasthenic syndrome caused by decreased agonist binding affinity due to a mutation in the acetylcholine receptor ε subunit. *Neuron.* 17:157–170.

Qin, F., A. Auerbach, and F. Sachs. 1996. Estimating single-channel kinetic parameters from idealized patch-clamp data containing missed events. *Biophys. J.* 70:264–280.

Schreiber, G., and A.R. Fersht. 1995. Energetics of protein-protein interactions: analysis of the barnase-barstar interface by single mutations and double mutant cycles. *J. Mol. Biol.* 248:478–486.

Sine, S.M., and A.G. Engel. 2006. Recent advances in Cys-loop receptor structure and function. *Nature.* 440:448–455.

Sine, S.M., and J.H. Steinbach. 1987. Activation of acetylcholine receptors on clonal mammalian BC3H-1 cells by high concentrations of agonist. *J. Physiol.* 385:325–359.

Sohn, J., and J. Rudolph. 2006. The energetic network of hotspot residues between Cdc25B phosphatase and its protein substrate. *J. Mol. Biol.* 362:1060–1071.

Taly, A., P.J. Corringer, T. Grutter, L. Prado de Carvalho, M. Karplus, and J.P. Changeux. 2006. Implications of the quaternary twist allosteric model for the physiology and pathology of nicotinic acetylcholine receptors. *Proc. Natl. Acad. Sci. USA.* 103:16965–16970.

Unwin, N. 2005. Refined structure of the nicotinic acetylcholine receptor at 4 Å resolution. *J. Mol. Biol.* 346:967–989.

Vaughan, C.K., A.M. Buckle, and A.R. Fersht. 1999. Structural response to mutation at a protein-protein interface. *J. Mol. Biol.* 286:1487–1506.

Wang, H.L., A. Auerbach, N. Bren, K. Ohno, A.G. Engel, and S.M. Sine. 1997. Mutation in the M1 domain of the acetylcholine receptor α subunit decreases the rate of agonist dissociation. *J. Gen. Physiol.* 109:757–766.

Wang, J., H.A. Lester, and D.A. Dougherty. 2007. Establishing an ion pair interaction in the homomeric rho1 γ-aminobutyric acid type A receptor that contributes to the gating pathway. *J. Biol. Chem.* 282:26210–26216.

Zhang, H., M. Skinner, W. Sandberg, A. Wang, and T. Terwilliger. 1996. Context dependence of mutational effects in a protein: the crystal structures of the V35I, I47V and V35I/I47V gene V protein core mutants. *J. Mol. Biol.* 259:148–159.